Paper Physics

Jérémie Viguié*, Saurabh Kumar, Bruno Carré and Laurent Orgéas

Enhancing the strength of tissue paper through pulp fractionation and stratified forming

https://doi.org/10.1515/npprj-2024-0058
Received August 19, 2024; accepted October 12, 2024;
published online October 29, 2024

Abstract: The potential of combining stratified paper forming with pulp fractionation was investigated to improve the balance between low density, which enhances water absorbency and softness, and the dry strength of tissue papers. The selected fractionation approaches allowed us to separate especially stiff, low-fibrillated fibers (A fractions) from flexible, fibrillated fibers containing fines (detached segments of fibers, fibrils, or lamellae fragments) (B fractions). After characterizing the morphological properties of each fiber fraction, 20 g/m^2 model papers were produced with and without wet pressing to tune the paper density. At a density of 0.3 g/cm^3, the tensile breaking stress of B papers was at least three times higher than that of A papers. The strain at break of B papers was also close to two times higher than that of A papers. Interestingly, bilayer papers A/B exhibited breaking stress values intermediate between those of A and B papers, while native pulp papers, *i.e.*, without fractionation and stratified forming, followed the trend of A papers. Notably, bi-layering the paper improved the breaking stress by up to twice as much without increasing the paper density, which could be highly beneficial in improving the balance of properties in tissue paper grades.

Keywords: stratified forming; pulp fractionation; mechanical strength; tissue paper

***Corresponding author: Jérémie Viguié**, Univ. Grenoble Alpes, CNRS, Grenoble INP, LGP2, F-38000, Grenoble, France; and Centre Technique du Papier (CTP), F-38044, Grenoble, France, E-mail: jeremie.viguie@lgp2.grenoble-inp.fr. https://orcid.org/0000-0002-8178-6257
Saurabh Kumar, Centre Technique du Papier (CTP), F-38044, Grenoble, France; and Now at Andritz Perfojet SAS, F-38330, Montbonnot, France
Bruno Carré, Centre Technique du Papier (CTP), F-38044, Grenoble, France
Laurent Orgéas, Univ. Grenoble Alpes, CNRS, Grenoble INP, 3SR Lab, F-38000, Grenoble, France. https://orcid.org/0000-0003-1668-688X

1 Introduction

Environmental and economic concerns are driving manufacturers of tissue papers to minimize the production resources (raw materials, energy, water…) while optimizing the end-use performances of these particular papers. Meanwhile, tissue papers require a combination of different properties to be increased and optimized: mechanical in-plane strength in both dry and wet states, water absorbency, out-of-plane bulk and surface softness's (De Assis et al. 2018). This optimization is complex and demands several challenges to be overcome. Indeed, the fiber web features that are optimal for providing high mechanical strength unfortunately greatly differ from those required for high absorbency and softness. For example, refining the pulp or adding of micro-fibrillated cellulose are known processing routes used to increase the in-plane strength of tissue papers by increasing the density of the fiber network and by improving bonding between fibers. However, in the same time, such forming techniques alter the absorbency and the (bulk and surface) softness of corresponding papers (Gigac and Fišerová 2008; Kullander et al. 2012; Morais et al. 2021a; Morais et al. 2021b; Viguié et al. 2022; Wang 2019; Zambrano et al. 2021). Paper creping acts in the opposite way by delaminating the fiber networks (thus by increasing their porosity and the out-of-plane softness) and by forcing the fiber bonds to be damaged/broken (thus by reducing both their in-plane stiffness and their yield strength) (De Assis et al. 2020).

Thus, to circumvent these bottlenecks and to make tissue grades with combined and optimized properties, stratified forming is a possible and relevant processing route which is followed for decades. This method consists in layering different pulps before dewatering using a stratified headbox (Lloyd 2000). Generally, two layers (rarely three) are superimposed. The first/inner layer may be made of long, flexible, highly fibrillated fibers and fines (which are detached segments of fibers, fibrils or lamellae fragments), to improve bonding and thus to provide strength. The second/outer layer(s) may be made of short, stiff and low fibrillated fibers to improve the surface softness as well as the water absorbency capacity (De Assis et al. 2018). Each pulp has a dedicated pulping, cleaning and refining process. Nevertheless, the

production cost could be further reduced by using a single type of pulp and by employing pulp fractionation to create distinct groups of fibers with different properties, which could then be used to form the stratified structure.

Indeed, stratified forming with prior pulp fractionation was proved to be a good way to optimize the compromise between the production cost and the mechanical performances of graphic papers (Harwood 1990; Huber et al. 2013; Oksanen et al. 2012). The controlled distribution of the different fiber fractions through the thickness of the structure by stratified forming has significantly improved the specific bending stiffness of these papers. Fractionation of pulp suspensions can be performed by pressure screening systems or hydrocyclone technologies. Screening systems equipped with finely perforated plates (either slots or holes) fractionate pulp suspensions based on the fiber length. Hydrocyclones fractionate the pulp on the basis of the stiffness and extent of development of fibers (related to wall thickness, coarseness and fibrillation), resulting from their different fiber migration behavior in the centrifugal flow field (Huber et al. 2018).

To date, no academic work has investigated the potential of stratified forming combined with pulp fractionation to improve the compromise of properties of tissue papers. This is the aim of this work: we examine the evolution of the structural and mechanical properties of model tissue papers processed with softwood kraft pulp, by using both fractionation approaches and stratification.

2 Material and methods

2.1 Native fiber pulp

The native paper pulp was a 100 % Northern Bleached Softwood Kraft Pulp (NBSK). It was slushed in a low consistency pulper (5 % consistency, 30 min, 45 °C). The pulp had an initial drainage index of 13°SR. No wet-end additives were used.

2.2 Pulp fractionation

As illustrated in Figure 1, we used two distinct fractionation approaches described hereafter.

2.2.1 First fractionation approach

The first approach (noted 1) consisted of a two-stage feed-forward hydrocyclone fractionation. The hydrocyclone fractionation is known to separate fibers following how they migrate in the centrifugal flow field: flexible fibrillated fibers and fines concentrate in the secondary vortex to be collected in the base part of the hydrocyclone while stiff and low fibrillated fibers concentrate in the primary flow to be collected in the apex part (Bergström 2006; Huber et al. 2018). This was achieved with an 80 mm head diameter industrial fractionating hydrocyclone (Kadant-NOSS AM80H). The two-stage feed forward fractionation was performed batch-wise, with the same single hydrocyclone being used for both the stages. Due to limited storage capacity, the first stage hydrocyclone base fraction was thickened on the pilot vacuum disc filter. The filter offers high fiber and fines retention. This thickened base fraction was added to the second stage base fraction to get a combined base fraction (noted B) and then thickened on the same vacuum filter. The other fraction, *i.e.*, the apex fraction (noted A), was collected and thickened using a laboratory centrifugation device, hence retaining all cellulosic elements. The fractionation parameters were carefully adjusted to achieve a 50 % dry mass for both the A and B fractions.

2.2.2 Second fractionation approach

The second approach (noted 2) consisted in separating the long fibers (LF) from the short ones (SF) by using an industrial pilot pressure screening system equipped with micro-holes basket (0.25 mm) and a 3-element solid core rotor (CTP, France). Long fibers are defined as those that do not pass through the screening system, while short fibers are those that do. Then each fraction was fractionated in a hydrocyclone. Four new fractions were collected (see Figure 1), *i.e.*, long, stiff and low fibrillated fibers (LFA), long flexible and highly fibrillated fibers (LFB), short stiff and less fibrillated fibers and fines (SFA), short flexible and highly fibrillated fibers and fines (SFB).

2.3 Manufacturing of model papers

Monolayered and stratified model papers were produced using an automated dynamic handsheet former (Techpap, Grenoble, France). The sheet was formed by the projection of pulp on a wire positioned on a rotating cylindrical jar. The wire was completely submerged in a water wall. The pulp projection was accomplished using an injector nozzle fixed on a delivery tube sweeping vertically up and down inside the rotating cylindrical jar. For the stratified model papers, each fraction was projected one after the other. A scoop system bailed out the water wall after the sheet was formed and the water remaining in the sheet was drained by centrifugal force. Sheets were all manufactured with a 20 ± 2 g/m^2 grammage together with a 0.652 ratio of jet speed/

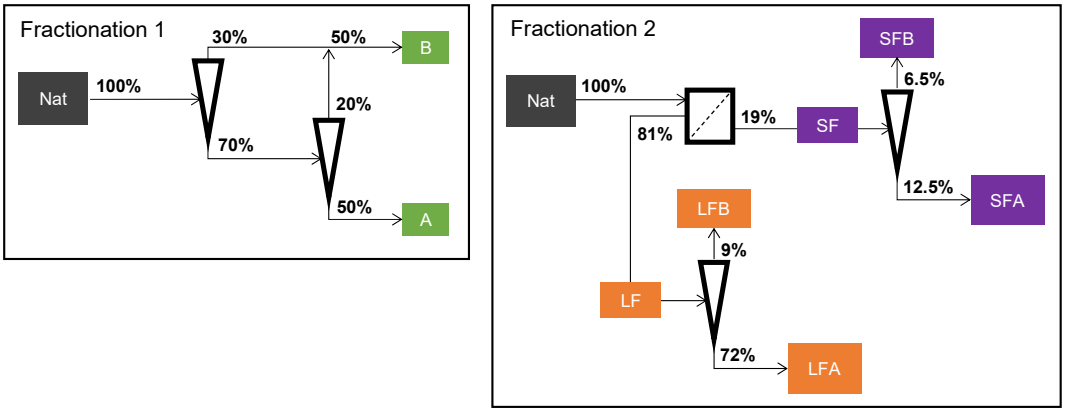

Figure 1: Schemes of the studied fractionation processes. Nat, native pulp; A, apex fraction; B, base fraction; LF, long fiber fraction; SF, short fiber fraction; LFA, long fiber apex fraction; LFB, long fiber base fraction; SFA, short fiber apex fraction and SFB, short fiber base fraction. The percentage corresponds to the proportion of dry mass for each obtained fraction.

wire speed (wire speed = 920 m/min), so that the fibers were preferentially oriented along the machine direction (MD) rather than along the cross direction (CD). The Sheets, with in-plane dimensions 880 × 240 mm^2, were slightly pressed to be removed from the wire using a cylindrical roll of 500 g. It is important to note that the longer dimension aligned with the MD, while the shorter dimension aligned with the CD. The sheets were then air-dried without any applied pressure, with the long edges sandwiched between PVC plates, leaving the short edges free.

To tailor the paper density, some of the handsheets were further pressed before drying on a roll press with a pressure of 60 N cm^{-1} (Techpap, France). They are referred to as "*P*" in the following. Note that the model papers were not creped. It might be an issue to conclude on the actual effects on the tissue paper (*i.e.*, creped paper). However, De Assis et al. (2020) recently found a reasonable correlation between the performances of uncreped and creped handsheets.

Two types of stratified papers have been made: the Stratified 1 with a layer of A fraction and a layer of B fraction, and the Stratified 2 with a layer of mixed LFA and SFA fractions and a layer of mixed LFB and SFB fractions in order to form two independent layers: one with stiff and low-fibrillated fibers and another with flexible, high-fibrillated fibers and fines. Each fraction was added according to its share in the entire pulp (Figure 1).

2.4 Characterization methods

2.4.1 Morphological properties of fibers

The morphological properties of fibers, namely the mean fiber length, the mean fiber width, the coarseness, the fine content and the macrofibrillation index, were measured with a Morfi fiber analyzer (Techpap, France) through image analysis. Note that the macrofibrillation index, which characterizes the external fibrillation of paper fibers, represents the ratio of total fibrils length to the total fiber+fibrils length (down to a scale of 3 µm). Fines are defined as elements with a length of less than 200 µm. Note that here fines were only generated during pulp production since the pulp was not refined (*i.e.*, they are "primary" fines).

2.4.2 Paper sheet physical properties

The paper sheet physical properties were assessed using the following standard methods: pre-conditioning (NF EN 20 187, 1993), basis weight (NF EN ISO 536, 1996), thickness adapted to tissue paper (ISO 12625-3) (Vieira et al. 2020) and dry tensile properties adapted to tissue paper (ISO 12625-4). This standard specifies a sample width of 50 mm and a testing speed of 50 mm/min. In our case, the sample length was set to 100 mm, as it was not possible to prepare samples of greater length. It should be noted that the testing conditions deviate from the assumption of pure uniaxial tension. As a result, the elastic modulus, calculated from the slope of the initial linear region of the stress-strain curve, should be considered as an apparent Young's modulus (noted *E*). Representative stress-strain curves for some model papers are presented in Figure 2.

2.4.3 Paper sheet microstructures

The microstructures of paper sheets were characterized using a field emission scanning electron microscope (FESEM, model Quanta 200 FEI) with an accelerating voltage of 10 kV. For that purpose, the samples were

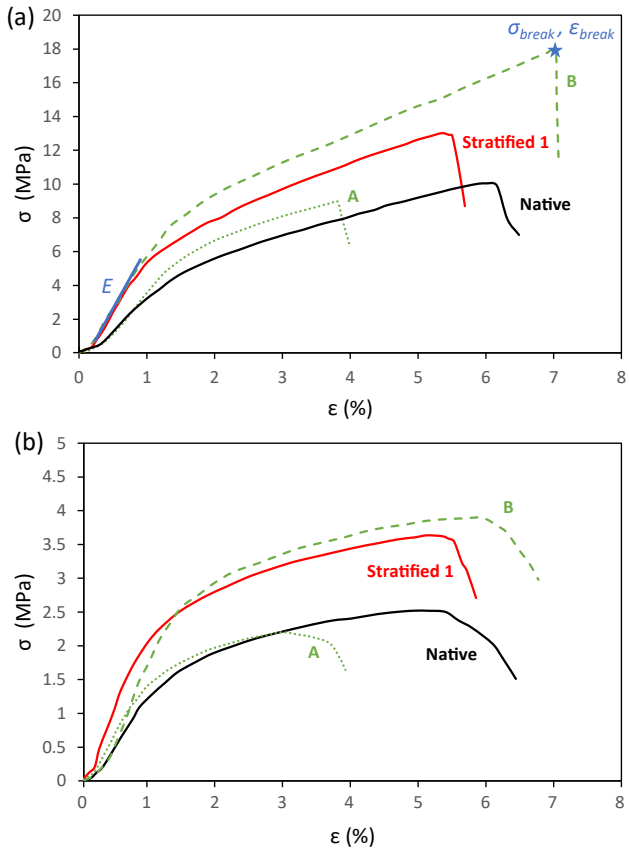

Figure 2: Representative stress-strain curves for selected model papers under pressed conditions, tested in (a) MD and (b) CD. *E* refers to the apparent Young's modulus, σ_{break} denotes the tensile breaking stress, and ε_{break} represents the strain at break.

mounted onto a substrate with carbon tape and coated with a thin layer of carbon.

3 Results and discussion

3.1 Structural properties of fibers and model papers

Table 1 reports the morphological properties of the Native and fractionated fibers following Approach 1. As expected, fraction B mainly gathered fibrillated fibers and fines. The external fibrillation of B fibers was twice as high as the external fibrillation of A fibers and the fines content was close to four times higher in fraction B. Besides, the fibers of fraction A were on average 25 % longer and 15 % thicker than the fibers of fraction B. Their coarseness was also 15 % higher. As a result, the fibers of fraction A were expected to be stiffer. Note that the morphological parameters of the native fibers were in between those reported for fractions A and B, as expected.

The structural properties of the model monolayered papers produced from fractions A and B are also reported in Table 1. The fraction B, *i.e.*, with more flexible and fibrillated fibers and a higher content of fines, formed 15 % thinner and thus denser fibrous networks, *i.e.*, 134 *vs.* 116 kg/m^3 or 288 *vs.* 265 kg/m^3 without or with pressing during the paper sheet fabrication, respectively. At fixed pressing condition, the densification as well as the development of bonding between fibers during drying are driven by capillary forces that arise from water which seek to minimize their liquid/air interface (Wohlert et al. 2021). The presence of small elements like fibrils and fines, as well as the ability of the fiber wall to deform, drastically increase the surface area subjected to capillary pressure and thus enhance the densification effect and fiber-to-fiber bonding (Hirn and Schennach 2015; Lindström et al. 2014). In addition, the densification of fibrous media with high polydispersity (because of the fine content) is also more efficient than that of more monodisperse media.

Table 2 presents the morphological parameters of fractionated fibers following Approach 2, alongside the structural properties of the related papers. As anticipated, fraction LF concentrated long, thick, and low-fibrillated fibers, whereas fraction SF concentrated short, thin, highly fibrillated fibers, along with fines. This distribution is visually depicted in Figure 3. On average, the fibers of fraction LF were twice as long and 20 % thicker compared to SF fibers. Additionally, the external fibrillation of SF fibers was at least twice as high as that of LF fibers, with SF containing at least six times more fines. The hydrocyclone fractionation process applied to each fraction resulted in fraction LFA, with the longest and thickest fibers, the lowest fibrillation index, and the lowest fines content. Consequently, fraction LFA formed the papers with the lowest densities (114 kg/m^3 (UP), 290 kg/m^3 (P)), while LF paper densities were only slightly higher (120 kg/m^3 (UP), 302 kg/m^3 (P)), consistent with the similarities in fiber morphological properties among these groups. Notably, the density of native paper approximated that of LFA papers (114 kg/m^3 (UP), 297 kg/m^3 (P)), a result which is possibly attributed to the complex structural properties of a web from mixed fibers. The density of such a web formed from a mixture of conformable and fibrillated fibers with stiff and low-fibrillated fibers could be limited by the stiffer furnish component (Fernandez and Young 1994; Niskanen and Kärenlampi 1998).

Fraction LFB was characterized by fibers with intermediate length and width, the lowest coarseness, and a relatively high fibrillation index. SFA fibers had mean length and width comparable to LFB but exhibited higher coarseness and a lower fibrillation index. Networks formed by LFB and SFA significantly differed in terms of density (156 *vs.* 124 kg/m^3 (UP), 381 *vs.* 319 kg/m^3 (P)), underscoring the

Table 1: Morphological properties of fibers of the native pulp, the apex fraction A, and the base fraction B, and physical properties of corresponding model monolayered papers made under wet unpressed (UP) or pressed (P) conditions.

Pulp properties		**Native**		**Fractionation 1**			
				A (50 %)		**B (50 %)**	
Fiber length *l* (µm)		1,298 ± 6		1,403 ± 12		1,098 ± 10	
Fiber width *w* (µm)		29.1 ± 0.1		32.4 ± 0.1		28.2 ± 0.1	
Aspect ratio *l*/*w*		45		43		39	
Coarseness (mg/m)		0.14 ± 0.01		0.15 ± 0.01		0.13 ± 0.01	
Fibrillation index (%)		0.35 ± 0.01		0.30 ± 0.01		0.62 ± 0.02	
Fines content (%)		2.4 ± 0.3		1.4 ± 0.1		5.5 ± 0.2	
Paper Properties		**UP**	**P**	**UP**	**P**	**UP**	**P**
Basis weight (g/m^2)		21.3 ± 0.2	21.6 ± 0.2	21.3 ± 0.5	20.7 ± 0.6	21.9 ± 0.4	23.5 ± 0.3
Thickness (µm)		187 ± 5	73 ± 3	184 ± 9	78 ± 4	164 ± 10	83 ± 7
Density (kg/m^3)		114 ± 4	297 ± 14	116 ± 8	265 ± 14	134 ± 9	288 ± 16
RBA (from Eq. (1))		0.07	0.11	0.07	0.08	0.07	0.20
Apparent Young's modulus *E* (GPa)	MD	0.19 ± 0.04	0.70 ± 0.10	0.17 ± 0.08	0.43 ± 0.12	0.13 ± 0.02	1.00 ± 0.06
	CD	0.05 ± 0.01	0.38 ± 0.08	0.06 ± 0.02	0.22 ± 0.04	0.05 ± 0.01	0.36 ± 0.01
Tensile breaking stress σ_{break} (MPa)	MD	1.84 ± 0.12	9.01 ± 0.67	1.89 ± 0.59	6.73 ± 0.67	5.09 ± 0.32	18.38 ± 0.86
	CD	0.67 ± 0.05	3.03 ± 0.25	0.52 ± 0.2	2.44 ± 0.21	1.20 ± 0.09	5.39 ± 0.22
Strain at break ε_{break} (%)	MD	3.6 ± 0.8	5.4 ± 1.3	2.9 ± 0.6	4.2 ± 0.7	5.9 ± 0.7	7.2 ± 1.1
	CD	3.8 ± 0.6	4.6 ± 0.4	2.3 ± 0.4	2.8 ± 0.6	3.7 ± 0.9	6.0 ± 0.9

substantial impact of fibrillation index and coarseness on paper density. Finally, SFB contained the shortest and thinnest fibers with the highest fibrillation index and fine content, resulting in the formation of paper with the highest density (218 kg/m^3 (UP), 435 kg/m^3 (P)). These observations align with existing literature, where densification is primarily driven by capillary forces during water removal. Specifically, a higher fibrillation index correlates with increased specific surface area and a decrease of the characteristic pore sizes, thus enhancing capillary forces and densification. Additionally, mean coarseness is inversely correlated with paper density. Greater coarseness is associated with thicker fiber walls, resulting in higher stiffness and ultimately, a less densely packed network.

Table 3 presents the average structural properties of the stratified papers. The mean density of these papers exhibited some variations compared to that of the Native paper, which is ascribed to different placements of the various fibrous elements during processing of the Native paper or the stratified ones. Specifically, it tended to be higher for Stratified 1 (A/B) paper under unpressed conditions (140 *vs.* 114 kg/m^3) and lower in the pressed configuration (267 *vs.* 297 kg/m^3), along with Stratified 2 (LFA+SFA/LFB+SFB) paper. FESEM images of the Stratified 1 paper are depicted in Figure 4. The two layers are distinctly visible, with fibers appearing more densely packed and bonded in the B fraction layer. Additionally, the formation of bridges composed of fibrils and fines between fibers is evident in the B layer. These observations correspond to the density contrast between the A and B papers. As already mentioned, the high polydispersity of the B fraction facilitates densification and bonding, while fibrils and fine elements increase the specific surface area exposed to capillary pressure, further enhancing these effects.

3.2 Mechanical properties of model papers

The profiles of the stress-strain curves were quite similar across different model papers (Figure 2). Initially, the curves exhibited a linear relationship between stress and strain, reflecting the material's elastic behavior. After reaching the yield point, stress continued to increase, albeit with a reduced slope, until the breaking point (represented as a star in Figure 2a). As expected, the curve typically shows a steeper slope in the MD compared to the CD and tends to gradually flatten as the paper deforms in the CD. In the following, the mechanical behavior of all model papers is compared based on the slope in the linear region, reflecting the apparent Young's modulus (E), the tensile breaking stress (σ_{break}) and the strain at break (ε_{break}).

Figure 5a and b depict the evolution of apparent Young's modulus with the paper density along the machine direction MD and cross direction CD, respectively. Notably, due to the used processing route which induced preferred fiber orientation along MD, the apparent Young modulus was

Table 2: Morphological properties of fibers of the long fibers fraction (LF), the long fibers apex fraction (LFA), the long fibers base fraction (LFB), the short fibers fraction (SF), the short fibers apex fraction (SFA) and the short fibers base fraction (SFB). Physical properties of model monolayered papers made under wet unpressed (UP) or pressed (P) conditions.

Pulp properties		**Fractionation 2**											
		LF (81 %)		**LFA (72 %)**		**LFB (9 %)**		**SF (19 %)**		**SFA (12.5 %)**		**SFB (6.5 %)**	
Fiber length *l* (µm)		1,537 ± 18		1,687 ± 8		977 ± 10		804 ± 4		981 ± 9		682 ± 4	
Fiber width *w* (µm)		30.8 ± 0.1		32.1 ± 0.1		26.4 ± 0.1		25.7 ± 0.1		28.3 ± 0.1		24.2 ± 0.2	
Aspect ratio *l*/*w*		50		53		37		31		35		28	
Coarseness (mg/m)		0.14 ± 0.01		0.16 ± 0.01		0.12 ± 0.01		0.14 ± 0.01		0.15 ± 0.01		0.13 ± 0.01	
Fibrillation index (%)		0.31 ± 0.01		0.27 ± 0.01		0.67 ± 0.01		0.68 ± 0.02		0.45 ± 0.01		0.91 ± 0.01	
Fines content (%)		1.3 ± 0.1		1.0 ± 0.0		4.5 ± 0.3		8.0 ± 0.1		3.5 ± 0.1		11.2 ± 0.2	
Paper properties		**UP**	**P**	**UP**	**P**	**UP**	**P**	**UP**	**P**	**UP**	**P**	**UP**	**P**
Basis weight (g/m^2)		22.2 ± 0.7	22.5 ± 0.4	20.3 ± 0.9	20.7 ± 0.1	22.6 ± 0.5	22.1 ± 0.8	21.5 ± 1.0	22.0 ± 1.0	21.3 ± 0.2	24.8 ± 1.1	22.8 ± 1.0	21.5 ± 0.6
Thickness (µm)		186 ± 5	76 ± 5	178 ± 9	72 ± 3	145 ± 5	58 ± 3	144 ± 7	64 ± 6	172 ± 10	78.2 ± 7	105 ± 12	50 ± 2
Density (kg/m^3)		120 ± 6	302 ± 16	114 ± 2	290 ± 14	156 ± 3	381 ± 16	149 ± 7	345 ± 18	124 ± 9	319 ± 13	218 ± 18	435 ± 22
RBA (from Eq. (1))		0.06	0.09	0.05	0.06	0.12	0.15	0.14	0.17	0.08	0.11	0.16	0.20
Apparent Young's modulus *E* (GPa)	MD	0.16 ± 0.03	0.61 ± 0.08	0.08 ± 0.01	0.43 ± 0.01	0.36 ± 0.02	0.96 ± 0.12	0.41 ± 0.07	0.99 ± 0.09	0.10 ± 0.03	0.59 ± 0.01	0.50 ± 0.06	1.21 ± 0.12
	CD	0.05 ± 0.01	0.43 ± 0.02	0.03 ± 0.00	0.16 ± 0.01	0.15 ± 0.01	0.53 ± 0.05	0.11 ± 0.03	0.51 ± 0.05	0.04 ± 0.01	0.23 ± 0.03	0.21 ± 0.02	0.52 ± 0.04
Tensile breaking stress σ_{break} (MPa)	MD	1.88 ± 0.06	8.45 ± 1.48	1.32 ± 0.07	6.68 ± 0.15	8.30 ± 0.38	28.08 ± 3.47	7.67 ± 0.51	25.30 ± 2.16	2.44 ± 0.41	9.19 ± 0.39	14.39 ± 0.53	36.98 ± 1.44
	CD	0.65 ± 0.05	3.04 ± 0.16	0.46 ± 0.04	2.31 ± 0.26	2.13 ± 0.26	7.15 ± 0.16	1.81 ± 0.22	5.85 ± 0.35	0.78 ± 0.02	3.64 ± 0.50	4.28 ± 0.28	9.76 ± 0.28
Strain at break ε_{break} (%)	MD	3.0 ± 0.6	3.6 ± 0.8	2.9 ± 0.7	4.6 ± 0.6	5.9 ± 0.6	7.2 ± 0.4	6.5 ± 0.6	7.8 ± 0.7	5.5 ± 1.0	5.8 ± 1.4	7.0 ± 2.0	6.5 ± 0.9
	CD	3.4 ± 0.4	3.0 ± 0.2	3.8 ± 0.7	4.1 ± 0.8	6.1 ± 0.9	6.3 ± 0.3	5.8 ± 0.8	5.2 ± 0.8	5.5 ± 0.9	4.9 ± 0.5	5.6 ± 1.1	5.6 ± 1.1

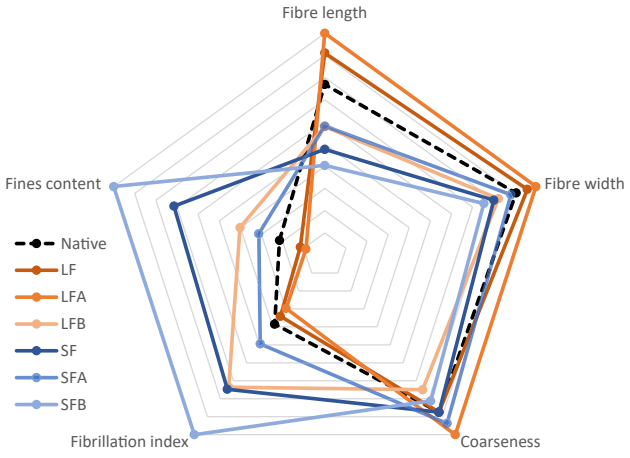

Figure 3: Comparison of the dimensionless morphological property for native pulp elements and the different fractionized pulps obtained from Approach 2. Each dimensionless property value was calculated as the ratio of the value for the respective fraction to the highest measured value.

observed to be around twice as high in MD compared to CD, whatever the considered paper. Firstly, the elastic moduli exhibited an overall increase with the paper density which is a well-known trend. At fixed paper formulation and whatever the considered formulation, this is emphasized by closely looking at investigated pressing conditions: the higher the normal stress during the forming phase, the higher the number of fiber-fiber contacts, the higher the contact surfaces (and thus the relative bonded area *RBA*) and the higher the Young's moduli (Marulier et al. 2015; Orgéas et al. 2021). However, some differences arise among the studied papers. At fixed pressing condition, these differences may be induced by the fiber aspect ratio l/w as well as the relative bonded area *RBA* (Page and Seth 1980, Orgéas et al. 2021). For example, following Page and Seth, the Young modulus E_p of an in-plane isotropic paper fiber network is a function of the fiber volume fraction ϕ, the fiber aspect ratio l/w, and the *RBA* as follows:

$$E_p = \frac{1}{3}E_f\phi\left(1 - \frac{1}{\frac{l}{w}RBA}\sqrt{\frac{E_f}{2G_f}}\right) \quad (1)$$

Where E_f and G_f are the fiber Young's and shear moduli, respectively. In the following these quantities were assumed constant regardless of fiber morphology, for the sake of simplicity. Eq. (1) shows that at given fiber volume fraction, the higher the fiber aspect ratio l/w or the *RBA*, the higher the Young modulus, with a limit which tends to that predicted by the Cox model (Cox 1952).

As evident from Figure 5, the model papers originating from the apex fiber fractions occupy the lower part of the cloud of experimental points, whereas those from the base fiber fractions were situated in the upper part. Meanwhile, the fiber aspect ratio l/w is higher for the apex fraction papers (refer to Tables 1 and 2). Therefore, according to Eq. (1), the evolution of this parameter alone cannot elucidate the observed difference in the evolution of apparent Young's moduli with paper density between apex and base fraction papers. It is more likely that the *RBA* could play a dominant role in this regard. The *RBA* was anticipated to be notably higher for the base fraction papers due to their

Table 3: Physical Properties of the two stratified papers made under (wet) unpressed (UP) or pressed (P) conditions. [e]() Estimations of the σ_{break} using a two-layer parallel model, by averaging the σ_{break} of the A fraction paper and the B fraction paper, taking into account the respective thickness of each layer.

Paper properties		Monolayered		Stratified 1		Stratified 2	
		Native		A/B (50 %/50 %)		LFA+SFA/LFB+SFB (84.5 %/15.5 %)	
		UP	P	UP	P	UP	P
Basis weight (g/m^2)		21.3 ± 0.2	21.6 ± 0.2	22.1 ± 0.2	22.4 ± 0.2	20.2 ± 0.9	21.7 ± 0.6
Thickness (µm)		187 ± 5	73 ± 3	158 ± 5	84 ± 5	185 ± 14	80 ± 8
Density (kg/m^3)		114 ± 4	297 ± 14	140 ± 7	267 ± 9	109 ± 6	273 ± 28
Apparent Young's modulus E (GPa)	MD	0.19 ± 0.04	0.70 ± 0.10	0.33 ± 0.08	0.83 ± 0.10	0.16 ± 0.04	0.62 ± 0.10
	CD	0.05 ± 0.01	0.38 ± 0.08	0.10 ± 0.01	0.25 ± 0.05	0.08 ± 0.01	0.24 ± 0.06
Tensile breaking stress σ_{break} (MPa)	MD	1.84 ± 0.12	9.01 ± 0.67	4.63 ± 0.41 [e](3.40)	13.60 ± 0.73 [e](12.74)	2.02 ± 0.12	9.08 ± 0.45
	CD	0.67 ± 0.05	3.03 ± 0.25	1.13 ± 0.04 [e](0.84)	3.78 ± 0.30 [e](3.96)	0.79 ± 0.02	3.01 ± 0.12
Strain at break ε_{break} (%)	MD	3.6 ± 0.8	5.4 ± 1.3	4.3 ± 0.9	5.2 ± 0.1	3.3 ± 0.3	4.1 ± 0.4
	CD	3.8 ± 0.6	4.6 ± 0.4	3.5 ± 0.3	5.1 ± 0.3	2.5 ± 0.2	3.7 ± 0.5

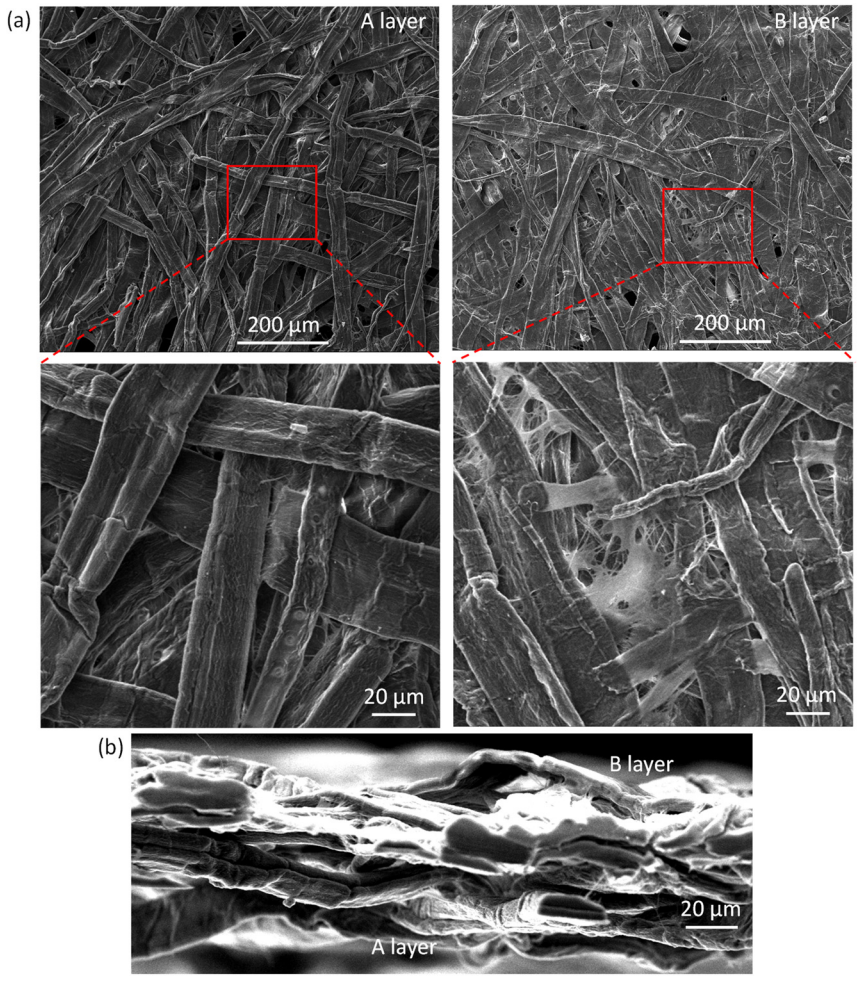

Figure 4: FESEM micrographs of stratified 1(A/B) paper: (a) A and B surfaces, and (b) cross section.

concentration of highly fibrillated fibers and fines. To verify this assumption, we estimated the *RBA* using Eq. (1) for all the monolayered model papers. For that purpose, the Young's modulus E_p was calculated as the mean value between the MD and CD, with E_f and G_f set to 30 GPa and 3 GPa respectively, *i.e.*, reasonable estimates for softwood fibers (Mansour et al. 2019; Orgéas et al. 2021). The resulting values of the *RBA* are reported in Tables 1 and 2, and plotted as functions of the paper densities in Figure 6. It is worth noting that this estimated *RBA* should not be considered strictly as a quantification parameter; rather, it should only be used as a tool for comparing papers in terms of degree of bonding.

As revealed by Figure 6, the *RBA* values exhibit significant variations among the different model papers and forming conditions. Firstly, for unpressed papers, *i.e.*, for identical pressing condition, the increase of the *RBA* with the paper density is noticeable, with, the lowest values for LFA, with slightly higher values for LF, then for apex fractions SFA and A, and with considerably higher values for SF and base fractions LFB, B, and SFB (up to four times higher than LFA for SFB). Interestingly, this ranking well correlates with the fibrillation index and fine content: the higher the values of these parameters, the higher the *RBA*. This relationship is expected, as the fibrillation index is associated with the specific surface area of fibers, which, along with the presence of fines, plays a pivotal role in bonding development. Notably, the native paper was situated in the upper part of the apex fraction group. In addition, it is worth noting that for a given model paper, increasing the normal pressing stress during paper forming induces an important increase of the paper density but also a noticeable increase of its *RBA* (Marulier et al. 2015; Orgéas et al. 2021).

Figure 7 illustrates the evolution of strain at break ε_{break} with paper density. ε_{break} is relatively equivalent in the MD and CD across all papers. This could be attributed to the specific drying conditions (air-dried and sandwiched between PVC plates along the long edges). However, ε_{break} depends on the considered fractions, albeit showing only a slight dependency/increase with the paper density (at fixed fraction). At fixed pressing condition, two distinct groups emerged: LF and apex fraction papers, which reached values

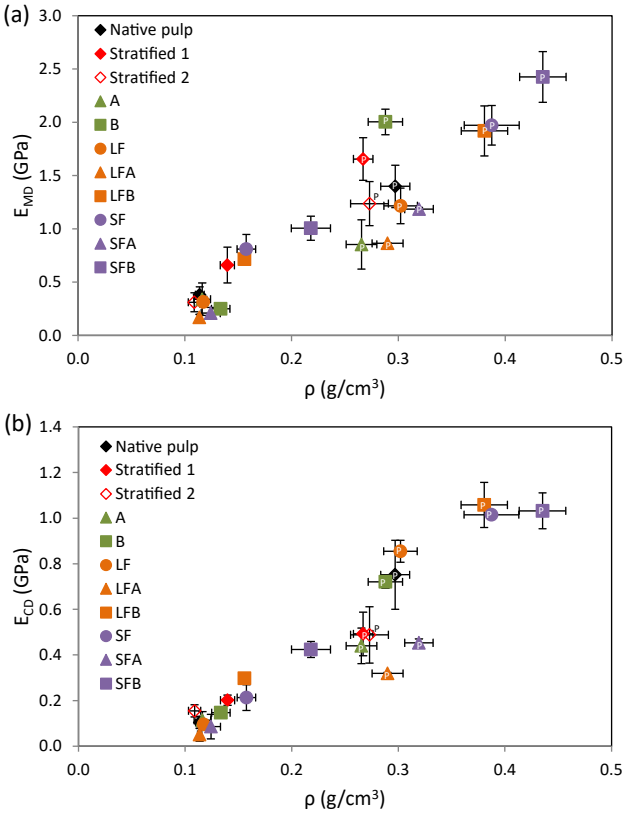

Figure 5: Apparent Young's moduli E_{MD} (a) and E_{CD} (b) as functions of the paper density ρ for all model papers along the machine (a) and cross (b) directions. Marks with a letter "P" indicate papers that were pressed upon processing.

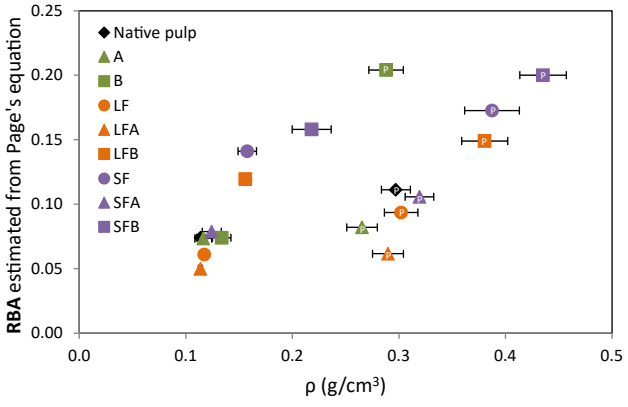

Figure 6: Relative bonded area RBA estimated from Eq. (1) as a function of paper density ρ for all the monolayered model papers. Marks with a letter "P" indicate papers that were pressed upon processing.

between 3 % and 5 %, and SF and base fraction papers, which reached values around 6–7 %. This trend appears to correlate well with the fibrillation index and fine content, and consequently, with *RBA*: higher values of these parameters corresponded to higher strain at break. The deformability of

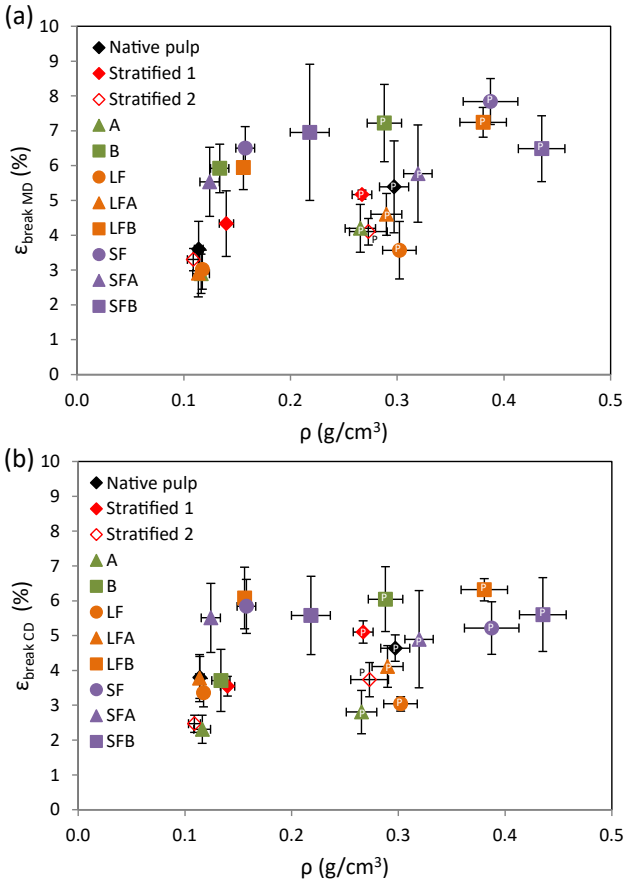

Figure 7: Strain at break ε_{break} as a function of the paper density ρ for all model papers in the (a) machine direction MD and (b) cross direction CD. Marks with a letter "P" indicate papers that were pressed upon processing.

low-density papers is known to largely depend on the bonding between fibers: the higher the bonding efficiency, the greater the strain at break (Kouko et al. 2020; Vishtal and Retulainen 2014). Notably, the native paper and the stratified papers occupied intermediate positions between the two groups. Note that the strain at break values in this study differ from those of industrial tissue papers, which typically exhibit higher values in the machine direction due to the creping process. It will be important to verify whether the differences between fractions remain consistent after the creping process.

Figure 8a and b shows the evolution of the tensile breaking stress σ_{break} of model papers with paper density, along the MD and CD, respectively. These results emphasize a well-known trend, whatever the fraction and the forming condition: the higher the paper density, the higher the number and the surface of contacts between particles (fibers, fines, fibrils), and thus the higher the stress levels required to damage and break the paper. Interestingly,

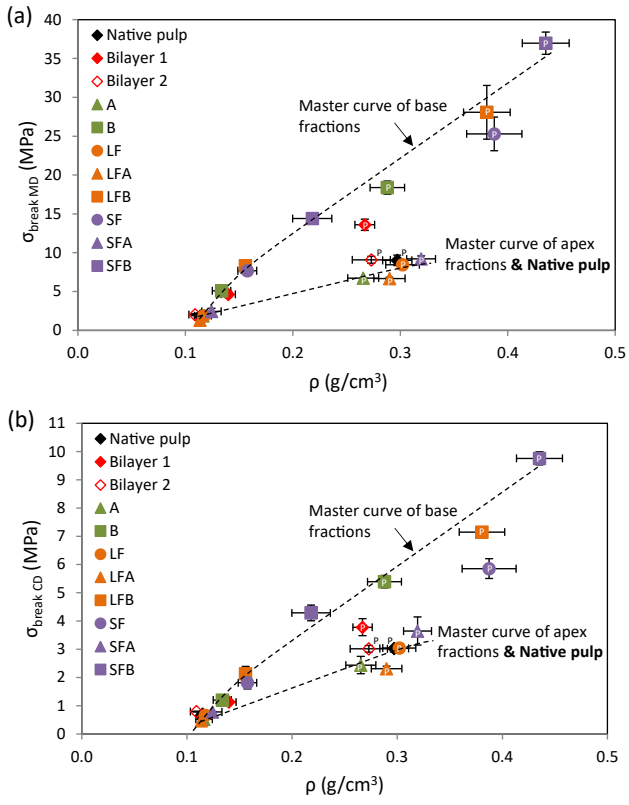

Figure 8: Evolution of the tensile breaking stress σ_{break} with the paper density ρ for all model papers along the machine (a) and cross (b) directions. Marks with a letter "P" indicate papers that were pressed upon processing.

papers from the base fractions and apex fractions follow two distinct curves. The breaking stress σ_{break} of base fraction papers exhibit a strong increase with paper density, whereas this property for apex fraction papers increased more gradually. For example, at a density of 0.3 g/cm^3, the σ_{break} of base fraction papers is at least twice that of apex fraction papers. This difference may be attributed to the higher level of fiber-to-fiber bonding in base fraction papers, as suggested by the estimated *RBA* reported in Figure 6. Fibrils and fines bridges which were formed between fibers in base fraction papers, as observed in Figure 4, contribute to carry the tensile load and to reduce stress concentrations in bonded regions (Motamedian et al. 2019). Also, it is noteworthy that LF papers tend to align with the master curve of apex fraction papers, while SF papers tend to align with the master curve of base fraction papers. This alignment was expected, as the short fiber fraction concentrates more fibrillated fibers and fines.

Interestingly, Stratified 1 papers occupied an intermediate position between the two aforementioned master curves (Figure 8), while the σ_{break} of native papers tended to align with the master curve of apex fraction papers. Ultimately, the σ_{break} of Stratified 1 paper surpassed that of both native and apex fraction papers by approximately 60 % according to the master curve analysis. This improvement underscores the effectiveness of stratification in overcoming the alignment of native paper behavior with that of apex fraction papers. It is worth mentioning that Stratified 2 papers remained within the same range as native papers, likely due to the distribution of each fraction in the stratified structure (84.5 % apex fraction fibers and 15.5 % base fraction fibers.

As previously mentioned, the native paper web can be regarded as a blend of stiff, low-fibrillated fibers and conformable, fibrillated fibers. The mechanical behavior of this web might differ from the average behavior of both the apex fraction paper and the base fraction paper. This difference arises because the development of bonding between fibers may be constrained by the stiffer, low-fibrillated fibers (Fernandez and Young 1994; Niskanen and Kärenlampi 1998). In this context, the stiff and low-fibrillated fibers could dictate the in-plane mechanical behavior of the native papers, resulting in behavior akin to that of apex fraction papers. However, by stratifying the sheet, the paper's mechanical performance was no longer hindered by the stiff, low-fibrillated fibers. Two webs, each approximately 10 g/m^2 and with relatively independent structural and mechanical properties, were superimposed (see Figure 4b). This hypothesis on the relative independency is supported by the estimations of σ_{break} using a two-layer parallel model based on the Voigt approximation (Aboudi 2013), as presented in Table 3 under "e", which are rather close to the experimental values.

4 Conclusions

In this experimental study, we investigated the potential of stratified forming combined with pulp fractionation to improve the mechanical strength of 20 g/m^2 model papers made from softwood kraft pulp. Pulp fractionation enabled the separation of fibers based on their morphology, fibrillation degree and fine content, resulting in papers with distinct mechanical behaviors. Regarding the strain at break ε_{break} and breaking stress σ_{break}, two distinct groups of papers emerged: papers made from short and/or flexible highly fibrillated fibers containing fines (B) and papers made from long and/or stiff low-fibrillated fibers (A). The breaking stress of B papers exhibited a strong increase with paper density whereas this property for A papers increased more gradually. Finally, at a density of 0.3 g/cm^3, the values σ_{break} of B papers is at least twice that of A papers. The strain at break of B papers was close to two times higher than that recorded for A papers albeit showing only a slight

dependency/increase with the paper density. This difference was primarily attributed to the level of fiber-to-fiber bonding, which is related to the specific surface area provided by fibrillated fibers and the presence of fines, both of which play a pivotal role in bonding development. Interestingly, regarding the breaking stress of the bilayer papers (A/B) were in an intermediate position between the two aforementioned trends while the native pulp paper (*i.e.*, without fractionation and stratified forming) followed the trend of A papers. As a result, bi-layering the paper improved σ_{break} up to twice as much without increasing the paper density. Since densification directly impacts the absorbency and softness of tissue paper, this approach could significantly improve the balance of properties across different tissue paper grades. Further investigations are required to quantify how this method influences these properties, as well as wet strength. Additionally, it is essential to assess whether the improvements in property balance are maintained after the creping process and to understand how stratification may affect the creping process itself. Finally, evaluating the potential of this method with hardwood or eucalyptus fiber pulps would be highly valuable.

Acknowledgments: Christian Berek, Priscilla Marquet, Mélanie Lehmann and Xavier Rousset are thanked for experimental work.

Research ethics: Not applicable.

Informed consent: Not applicable.

Author contributions: All authors have accepted responsibility for the entire content of this manuscript and approved its submission.

Use of Large Language Models, AI and Machine Learning Tools: GPT-4 was used to enhance the language in certain sections.

Conflict of interest: The authors states no conflict of interest.

Research funding: The authors acknowledge the financial support from CTP and CTPi Members. LGP2 and 3SR Lab are part of the LabEx Tec 21 and the Carnot Institute Polynat.

Data availability: The authors confirm that the data supporting the findings of this study are available within the article.

References

Aboudi, J. (2013). *Mechanics of composite materials: a unified micromechanical approach*. Elsevier, Amsterdam.

Bergström, J. (2006). *Flow field and fiber fractionation studies in hydrocyclones*, Doctoral dissertation. KTH, Stockholm.

Cox, H.L. (1952). The elasticity and strength of paper and other fibrous materials. *Br. J. Appl. Phys.* 3: 72–79, https://doi.org/10.1088/0508-3443/3/3/302.

De Assis, T., Reisinger, L.W., Pal, L., Pawlak, J., Jameel, H., and Gonzalez, R.W. (2018). Understanding the effect of machine technology and cellulosic fibers on tissue properties–A review. *BioResources* 13: 4593–4629, https://doi.org/10.15376/biores.13.2.deassis.

De Assis, T., Pawlak, J., Pal, L., Jameel, H., Reisinger, L.W., Kavalew, D., Campbell, C., Pawlowska, L., and Gonzalez, R.W. (2020). Comparison between uncreped and creped handsheets on tissue paper properties using a creping simulator unit. *Cellulose* 27: 5981–5999, https://doi.org/10.1007/s10570-020-03163-0.

Fernandez, E.O. and Young, R.A. (1994). An explanation for the deviation from linearity in properties of blends of mechanical and chemical pulps. *Tappi J.* 77: 221–224.

Gigac, J. and Fišerová, M. (2008). Influence of pulp refining on tissue paper properties. *Tappi J.* 7: 27–32, https://doi.org/10.32964/tj7.8.27.

Harwood, J.W. (1990). Stratification of paper grades. *Tappi J.* 73: 115–122.

Hirn, U. and Schennach, R. (2015). Comprehensive analysis of individual pulp fiber bonds quantifies the mechanisms of fiber bonding in paper. *Sci. Rep.* 5: 1–9, https://doi.org/10.1038/srep10503.

Huber, P., Carré, B., Fabry, B., and Kumar, S. (2013). Optimizing stratified forming for light-weight coated paper grades made from deinked pulp fractions. *Nord. Pulp Pap. Res. J.* 28: 302–312, https://doi.org/10.3183/npprj-2013-28-02-p302-312.

Huber, P., Carré, B., Kumar, S., and Lecourt, M. (2018). Optimum strategies for pulp fractions refining. *Nordic Pulp Paper Res. J.* 33: 3–11, https://doi.org/10.1515/npprj-2018-3012.

Kouko, J., Turpeinen, T., Kulachenko, A., Hirn, U., and Retulainen, E. (2020). Understanding extensibility of paper: role of fiber elongation and fiber bonding. *Tappi J.* 19: 125–135, https://doi.org/10.32964/tj19.3.125.

Kullander, J., Nilsson, L., and Barbier, C. (2012). Evaluation of furnishes for tissue manufacturing; suction box dewatering and paper testing. *Nordic Pulp Paper Res. J.* 27: 143–150, https://doi.org/10.3183/npprj-2012-27-01-p143-150.

Lindström, T., Fellers, C., Ankerfors, M., and Glad-Nordmark, G. (2014). On the strength mechanism of dry strengthening of paper with nanocellulose. In: *Proceedings of the recent advances in cellulose nanotechnology research: production, characterization and applications*. Trondheim Symposium, Trondheim, Norway.

Lloyd, M. (2000). Stratified (multilayer) forming: a technology for the new millennium? *Appita J.* 53: 188–194.

Mansour, R., Kulachenko, A., Chen, W., and Olsson, M. (2019). Stochastic constitutive model of isotropic thin fiber networks based on stochastic volume elements. *Materials* 12: 538.

Marulier, C., Dumont, P.J.J., Orgéas, L., Rolland du Roscoat, S., and Caillerie, D. (2015). 3D analysis of paper microstructures at the scale of fibres and bonds. *Cellulose* 22: 1517–1539.

Morais, F.P., Carta, A.M.M., Amaral, M.E., and Curto, J.M. (2021a). Cellulose fiber enzymatic modification to improve the softness, strength, and absorption properties of tissue papers. *BioResources* 16: 846–861, https://doi.org/10.15376/biores.16.1.846-861.

Morais, F.P., Carta, A.M., Amaral, M.E., and Curto, J.M. (2021b). Micro/nanofibrillated cellulose (MFC/NFC) fibers as an additive to maximize eucalyptus fibers on tissue paper production. *Cellulose* 28: 1–19, https://doi.org/10.1007/s10570-021-03912-9.

Motamedian, H.R., Halilovic, A.E., and Kulachenko, A. (2019). Mechanisms of strength and stiffness improvement of paper after PFI refining with a focus on the effect of fines. *Cellulose* 26: 4099–4124, https://doi.org/10.1007/s10570-019-02349-5.

Niskanen, K. and Kärenlampi, P. (1998). In-plane tensile properties. *Paper Phys.* 16: 172.

Oksanen, A., Salminen, K., Kouko, J., and Retulainen, E. (2012). The effects of TMP and filler stratifying on wet web runnability and end product quality of fine paper. *Nord. Pulp Pap. Res. J.* 27: 130–136, https://doi.org/10.3183/npprj-2012-27-01-p130-136.

Orgéas, L., Dumont, P.J., Martoïa, F., Marulier, C., Le Corre, S., and Caillerie, D. (2021). On the role of fiber bonds on the elasticity of low-density papers: a micro-mechanical approach. *Cellulose* 28: 9919–9941, https://doi.org/10.1007/s10570-021-04098-w.

Page, D.H. and Seth, R.S. (1980). The elastic modulus of paper. II: the importance of fiber modulus, bonding, and fiber length. *Tappi* 63: 113–116.

Vieira, J.C., de Oliveira Mendes, A., Carta, A.M., Galli, E., Fiadeiro, P.T., and Costa, A.P. (2020). Impact of embossing on liquid absorption of toilet tissue papers. *BioResources* 15: 3888–3898, https://doi.org/10.15376/biores.15.2.3888-3898.

Viguié, J., Kumar, S., and Carré, B. (2022). A comparative study of the effects of pulp fractionation, refining, and microfibrillated cellulose addition on tissue paper properties. *BioResources* 17: 1507–1517, https://doi.org/10.15376/biores.17.1.1507-1517.

Vishtal, A. and Retulainen, E. (2014). Boosting the extensibility potential of fiber networks: a review. *BioResources* 9: 7951–8001, https://doi.org/10.15376/9.4.7951-8001.

Wang, Y. (2019). *The physical aspects of softness perception and its relationship to tissue paper properties*. North Carolina State University, Raleigh, NC.

Wohlert, M., Benselfelt, T., Wågberg, L., Furó, I., Berglund, L.A., and Wohlert, J. (2021). Cellulose and the role of hydrogen bonds: not in charge of everything. *Cellulose* 29: 1–23, https://doi.org/10.1007/s10570-021-04325-4.

Zambrano, F., Wang, Y., Zwilling, J.D., Venditti, R., Jameel, H., Rojas, O., and Gonzalez, R. (2021). Micro-and nanofibrillated cellulose from virgin and recycled fibers: a comparative study of its effects on the properties of hygiene tissue paper. *Carbohydr. Polym.* 254: 117430, https://doi.org/10.1016/j.carbpol.2020.117430.